INTERNATIONAL SOCIETY FOR SOIL MECHANICS AND GEOTECHNICAL ENGINEERING

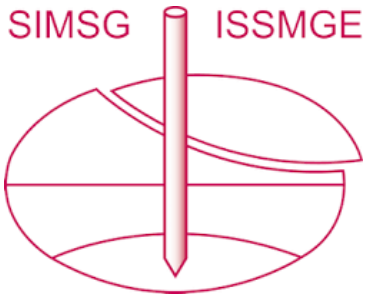

This paper was downloaded from the Online Library of the International Society for Soil Mechanics and Geotechnical Engineering (ISSMGE). The library is available here:

https://www.issmge.org/publications/online-library

This is an open-access database that archives thousands of papers published under the Auspices of the ISSMGE and maintained by the Innovation and Development Committee of ISSMGE.

The paper was published in the proceedings of the 10th European Conference on Numerical Methods in Geotechnical Engineering and was edited by Lidija Zdravkovic, Stavroula Kontoe, Aikaterini Tsiampousi and David Taborda. The conference was held from June 26th to June 28th 2023 at the Imperial College London, United Kingdom.

To see the complete list of papers in the proceedings visit the link below:

https://issmge.org/files/NUMGE2023-Preface.pdf

Proceedings 10th NUMGE 2023
10th European Conference on Numerical Methods in Geotechnical Engineering
Zdravkovic L, Kontoe S, Taborda DMG, Tsiampousi A (eds)

© Authors: All rights reserved, 2023
https://doi.org/10.53243/NUMGE2023-230

Numerical analysis of the axially loaded piles in sand by considering soil-pile interaction

M. Saberi[1], B.W. Byrne[1], H.J. Burd[1]

[1]*Department of Engineering Science, University of Oxford, Oxford, UK*

ABSTRACT: Numerical simulation of shaft resistance in axially loaded piles has been a key subject in geotechnical designs. In this study, the application of a numerical modelling approach so-called Hybrid-Winkler-Interface (HWI) for simulating pile behaviour in sands under axial load is studied. The HWI is a hybrid formulation including beam elements, Winkler springs and a layer of solid thin-layer interface element formulated in a bounding surface and critical state soil mechanics framework. The HWI input parameters have physical meanings, and they can be calibrated using standard shear tests. The approach can simulate complex behaviours in soil-pile interaction systems including: hardening/softening, compaction/dilation, accumulative contraction, and stress degradation. In this study, the frictional resistance of soil-pile systems embedded in sands with different densities and surface roughness under axial loads with different amplitudes are numerically simulated by considering advanced soil-pile interface effects. The numerical predictions are verified against available observations published in the literature.

Keywords: Shaft resistance; Axial loading; Hybrid-Winkler-Interface; Soil-pile interaction

1 INTRODUCTION

Piles are widely employed as the foundations in different geo-structures including tall buildings, bridges, offshore drilling platforms, and offshore wind power jacket structures. Pile foundations may experience monotonic and cyclic axial loads during their operational lifetimes. For example, overhead traffic in viaducts and overturning moments caused by winds and waves in offshore jacket foundations are mainly transferred to the piles via axial loading (Zhou et al., 2019). The shaft resistance of an axially loaded pile may experience hardening/softening, and compaction/dilation under monotonic loading conditions, and stress degradation and stabilization under cyclic loading conditions (Jardine and Standing, 2012; Randolph, 2003; Saberi et al., 2018); these aspects should be considered in the design process. Thus, considerable attention has been given to predicting the mobilized and ultimate shaft resistance of axially loaded piles loads in geotechnical design.

Different studies have been conducted to predict the pile shaft friction under axial loads using analytical and semi-analytical techniques (Kraft et al., 1981; Merritt et al., 2012; Randolph and Wroth, 1978; Rollins et al., 2005), *t-z* spring models (Wang et al., 2020; Zhou et al., 2019), and monotonic soil-pile interface models (Lashkari, 2013). Analytical solutions are not capable of considering the effects of complex nonlinear stress-displacement behaviour and volumetric deformation of surrounding soils on shaft resistance. The other approaches are either for monotonic behaviour or incapable of capturing the effect of volumetric deformation of adjacent soil on the soil-pile interface behaviour. With advances in numerical methods and computational algorithms, it has been possible to employ two-dimensional (2D) and three-dimensional (3D) finite element (FE) analyses to more realistically simulate soil-pile interaction phenomena (Han et al., 2017; Loukidis and Salgado, 2008). However, the high computational cost and the need for sophisticated soil constitutive models limit the applicability of this approach for routine design. Thus, there is a need for a computationally efficient numerical modelling procedure capable of capturing advanced soil-pile interaction behaviour for axially loaded piles.

The mobilized and ultimate shaft resistance in soil-pile systems is mainly governed by the mechanical behaviour of a thin soil layer at the shaft-soil interface, and the volume constraints applied by the surrounding soil. This interface zone experiences volumetric compaction/dilation, accumulative contraction and stabilization, and even particle breakage under shear deformations; these aspects should be accounted for to obtain accurate prediction of shaft resistance (Saberi et al., 2018; Vafaei et al., 2021). With this aim, in the current study the shaft resistance of axially loaded piles under monotonic and cyclic loading is predicted using an efficient numerical modelling approach called 'Hybrid Winkler Interface' (HWI). The HWI model is verified by comparing the model predictions with available laboratory observations. The HWI model employs beam/solid elements for simulating pile, thin-layer interface elements for the soil-pile interface zone and Winkler springs for the surrounding soil. The HWI input parameters can be easily calibrated by standard shear tests, and this approach is simply integrated in finite element

codes. The HWI approach is capable of rapidly simulating (compared to 3D finite element methods) the hardening/softening and degradation of shaft resistance by considering the effects of volumetric compaction/dilation, accumulative contraction, and particle breakage.

2 HYBRID-WINKLER-INTERFACE (HWI)

The HWI modelling approach is a hybrid formulation consisting of beam/solid elements representing the pile, lateral Winkler springs representing the soil mass, and a layer of thin-layer solid interface elements to represent the soil-structure interface. This approach was recently adopted for buried pipelines analysis (Saberi et al., 2022); however, it has not yet been employed in soil-pile interaction systems. The HWI model proposed in this study simulates a 3D FE soil-pile systems by a 2D axisymmetric model as shown in Figure 1.

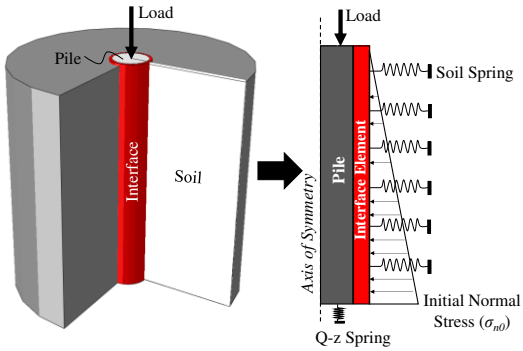

Figure 1. The proposed HWI approach for soil-pile system.

2.1 Soil spring and pile

The soil spring stiffness (K), which replicates the far-field stiffness around the pile, can be calculated as an elastic stiffness via cavity expansion theory (Boulon and Foray, 1986; Houlsby, 1991) and as a function of pile surface roughness (Jardine et al., 1998). In this study, it is suggested that K is determined by:

$$K = (4G/D)(R_n/R_{cr}) \quad (1)$$

where R_n is a normalized roughness ($R_n = R_{max}/D_{50}$), R_{cr} is the critical normalized roughness (usually 0.1 to 0.15), and R_{max} is the vertical distance between the maximum peak and minimum valley of the surface along a profile length of D_{50} (Uesugi and Kishida, 1986). D is the pile diameter and G is the soil shear modulus which is estimated by:

$$G = \alpha G_{max} \quad (2)$$

where α is suggested to be a value between 0.03 and 0.15 based on laboratory observations (Fioravante, 2002; Lehane et al., 2005), and G_{max} is the maximum small-strain shear modulus, which can be estimated using empirical relationships available in the literature. In this study, the Hardin and Richart (1963) relationship (Equation 3) was used for calculating the soil spring stiffness,

$$G_{max} = C_g\,(2.17 - e)^2/(1 + e)\,p'^{n_g} p_{ref}^{1-n_g} \quad (3)$$

where e is void ratio, p_{ref}=100 kPa is the reference pressure, p' is the mean effective stress, and C_g = 900 and n_g = 0.4 are constants suggested for Toyoura sand (Loukidis and Salgado, 2008).

The soil resistance at the pile tip is incorporated into the modelling approach using the API Q-z spring model (API, 2007). This model is adopted for the current purpose to give Equation (4),

$$Q_{max} = \sigma_{tip} N_q A_{tip} \quad (4)$$

where Q_{max} is the ultimate resistance of the Q-z spring, σ_{tip} is the overburden pressure at the pile tip, N_q is a bearing capacity factor, and A_{tip} is the area of the pile tip.

The pile can be simulated by beam or solid elements. In this study, linear elastic beam elements were utilized.

2.2 Soil-pile interface

In this study, the complex soil-pile interaction including shear and normal stress variations and volumetric deformations at the soil-pile interface zone is captured using solid thin-layer interface elements. These elements employ an advanced 2D state-dependent interface constitutive model in the framework of bounding surface plasticity and critical state soil mechanics CSSM (Saberi et al., 2017, 2019). This model was implemented in ABAQUS (Dassault Systèmes, 2014) using a user-subroutine 'UMAT' in conjunction with four-node quadrilateral isoparametric solid elements. Based on laboratory observations (e.g. Uesugi et al. 1986), the interface thickness of 2 mm and 1.4 mm are used here to simulate Fioravante (2002) and Wang et al. (2020) test data respectively. Interface thickness variation has negligible impact on the peak and residual shear strengths. Table 1 provides a summary of the constitutive formulations.

2.3 Boundary condition and loading

An initial normal stress (σ_{n0}) together with the soil spring stiffness is applied to the interface elements to simulate the soil confinement effects under shearing as illustrated in Figure 1. The σ_{n0} at different depths along the shaft is calculated by,

$$\sigma_{n0} = K_{lat}\gamma' z \quad (5)$$

where γ' is the soil effective unit weight, z is depth, and K_{lat} is the coefficient of lateral earth pressure.

The pile surface roughness affects the K_{lat} value; Loukidis and Salgado (2008) suggested the following relationship for K_{lat} in rough piles.

Table 1. Constitutive equations of the interface model and model parameters (Saberi et al. 2017, 2019).

Constitutive formulation	Eq.	Description	Parameters
Elasticity			
$\dot{\boldsymbol{\sigma}} = \boldsymbol{D}^e \dot{\boldsymbol{\varepsilon}}^e = \begin{bmatrix} D_{n0}\sqrt{\sigma_n/p_{atm}} & 0 \\ 0 & D_{t0}\sqrt{\sigma_n/p_{atm}} \end{bmatrix} \dot{\boldsymbol{\varepsilon}}^e$	(6)	▪ $\boldsymbol{D}^e$: elastic stiffness matrix ▪ p_{atm}: atmospheric pressure, given by 100 (kPa)	D_{n0} and D_{t0}
Elasto-plasticity			
Yield surface			
$f = (\mu - \alpha) \mp m = \frac{\tau}{\sigma_n} - \alpha - sm = 0$	(7)	▪ f: yield function (Lashkari, 2013) ▪ τ/σ_n: stress ratio (μ) ▪ α: back-stress-ratio ▪ m: control the yield surface size and it is $0.01\mu^{cs}$ to $0.05\mu^{cs}$	
$s = \begin{cases} +1 & \mu - \alpha \geq 0 \\ -1 & \mu - \alpha < 0 \end{cases}$	(8)		
Critical state			
$\psi = e - e_{cs}$	(9)	▪ ψ: state parameter ▪ e: void ratio at the current state ▪ e_{cs}: critical state (CS) void ratio ▪ W_p: modified plastic work ▪ $\langle\ \rangle$: Macaulay brackets; <x>= x if x>0, <x>= 0 if x≤0 ▪ τ^{cs} and σ_n^{cs}: shear and normal stress at CS ▪ μ^{cs}: CS surface slope in σ_n-τ plane (i.e. CS stress ratio)	e_{cs0}, λ, b_{r1}, b_{r2} and μ^{cs}
$e_{cs} = e_{cs0}(1 - \frac{W_p}{b_{r1} + b_{r2} W_p}) - \lambda \ln(\sigma_n/p_{atm})$	(10)		
$W_p = \int \left(\sigma_n \langle \dot{\varepsilon}_n^p \rangle + \tau \dot{\varepsilon}_t^p\right)$	(11)		
$\tau^{cs}/\sigma_n^{cs} = \mu^{cs}$	(12)		
Dilatancy			
$\mu^d = \mu^{cs}\, exp(K^d \psi)$	(13)	▪ μ^d: dilatancy stress ratio ▪ D: dilatancy coefficient ▪ Γ: loading index ▪ $\boldsymbol{R}$: direction of increment of plastic strain vector ▪ $\boldsymbol{n}$: vector normal to yield surface f ▪ K_p: plastic modulus ▪ $\mu < \mu^d$: contracting response (D>0) ▪ $\mu > \mu^d$: dilatant response (D<0) ▪ D=0: zero volumetric rate response ▪ $\boldsymbol{R} \neq \boldsymbol{n}$: non-associated flow rule	K^d and A^d
$\mathrm{D} = \dot{\varepsilon}_n^p / \left\lvert \dot{\varepsilon}_t^p \right\rvert = A^d(d^d) = A^d(\mu^d - s\mu)$	(14)		
$\dot{\boldsymbol{\varepsilon}}^{\mathrm{p}} = \begin{Bmatrix} \dot{\varepsilon}_n^p \\ \dot{\varepsilon}_t^p \end{Bmatrix} = \Gamma \boldsymbol{R}$	(15)		
$\Gamma = \boldsymbol{n}^T \dot{\boldsymbol{\sigma}} / K_p$	(16)		
$\boldsymbol{R} = \begin{Bmatrix} R_n \\ R_t \end{Bmatrix} = \begin{Bmatrix} D \\ \partial f/\partial \tau \end{Bmatrix} = \begin{Bmatrix} D \\ s \end{Bmatrix}$	(17)		
$\boldsymbol{n^T} = \{\partial f/\partial \sigma_n \ \ \partial f/\partial \tau\}$	(18)		
Plastic modulus			
$K_p = K_{p0} D_{t0} \sqrt{\sigma_n/p_{atm}}\ (\mu^f - s\mu)/\lvert\alpha\rvert$	(19)	▪ μ^f: failure or peak stress ratio ▪ $K_p > 0$: hardening behavior ▪ $K_p < 0$: softening behavior	K_{p0} and K^f
$\mu^f = \mu^{cs} exp(-K^f \psi)$	(20)		

$$K_{lat-R} = \frac{CK_0}{exp\,(0.2\sqrt{K_0 - 0.4}}\, exp\left\{\frac{D_r}{100}\left[1.3 - 0.2\, ln\left(\sigma'_{v0}/p_{ref}\right)\right]\right\} \quad (21)$$

where $K_{lat\text{-}R}$ is the coefficient of lateral earth pressure in piles with rough shafts, K_0 is at-rest coefficient lateral earth pressure, Dr (%) is soil relative density, and C is a model constant with a value around 0.7 as suggested by Loukidis and Salgado (2008). On the other hand, Kulhawy (1991) based on laboratory observations recommended $2/3K_0$ as the lower band of K_{lat} for smooth pile surfaces. In this study, the interpolation relationships suggested by Lashkari (2013) are used to consider the effect of surface roughness on K_{lat} as follows,

$$K_{lat} = \begin{cases} \frac{2}{3}K_0 + \left(K_{lat-R} - \frac{2}{3}K_0\right)\frac{R_n}{R_{cr}}, & R_n < R_{cr} \\ K_{lat-R}, & R_n \geq R_{cr} \end{cases} \quad (22)$$

3 MODEL CALIBRATION

In HWI modelling, calibrating the interface consitutive model plays the main role in the calibration process. The interface model requires eleven calibration parameters in total: two for elasticity (D_{t0} and D_{n0}), three for critical state (e_{cs0}, λ and μ^{cs}), two for dilatancy (A^d and K^d), one for failure (K^f), one for hardening (K_{p0}), and two for particle breakage (b_{r1} and b_{r2}). The parameters all have physical meanings and can be readily determined through standard interface shear tests: Constant Normal Load (CNL)/Constant Normal Stiffness (CNS) shear tests. The interface model parameters can be determined as described in detail in Saberi et al. (2017, 2019); however, for the sake of completeness, a brief explanation is provided here.

The D_{t0} and D_{n0} are evaluated using Equation (6) and by the initial slopes of the shear stress (τ)-tangential displacement (u_t) under CNL condition and normal stress (σ_n)-normal displacement (u_n) respectively. Alternatively, the elastic normal stiffness parameter D_{n0} can be taken as proportional to the elastic tangential stiffness parameter D_{t0}. A value of D_{n0}=1D_{t0} to 2D_{t0} results in good predictions in most interface systems (Saberi et al., 2020a, 2020b). If the shear stresses at critical state (τ_{cr}) are plotted against the corresponding normal stresses ($\sigma_{n\text{-}cr}$), the slope of the best fit line starting from the origin is obtained as μ^{cs}. For capturing e_{cs0} and λ, one can plot the critical void ratios (e_{cr}) at different σ_n against $\ln(\sigma_n/p_{atm})$. The slope of the best fit line of the points represents λ and the intersection of the fit line with the e_{cr} axis is given as e_{cs0}.

The parameter A^d is determined using the data of monotonic interface shear tests in u_n-u_t plane. u_n=ε_n×t and u_t=ε_t×t in which t is the interface thickness. Assuming the elastic parts of u_n and u_t are negligible, the following equation is drawn from Equation (14).

$$A^d \approx (du_n/|du_t|)/(\mu^d - \mu) \qquad (23)$$

Using Equation (23), different values of A^d are calculated through the data obtained from CNL/CNS tests. The average value of A^d is recommended for use in the interface model.

Using the data at phase transformation and failure (i.e. peak) states, the parameters K^d and K^f are calculated from Equations (24-25):

$$K^d = ln(\mu^d/\mu^{cs})/\psi_{phts} \qquad (24)$$

$$K^f = ln(\mu^f/\mu^{cs})/-\psi_f \qquad (25)$$

where ψ_{phts} and ψ_f are state parameters at phase transformation and failure (i.e. peak) states. Thus, K^d and K^f can be determined as the slope of the best fit line passing through the origin by plotting ψ_{phts} against $\ln(\mu^d/\mu^{cs})$ and ψ_f against $-\ln(\mu^f/\mu^{cs})$ respectively at different CNL/CNS shear tests.

The parameter K_{p0} can be easily estimated by a trial and error or it can be shown that the following relation for an interface under CNL condition can be drawn:

$$d\varepsilon_t = (1/D_t + 1/K_p)d\tau \qquad (26)$$

By substituting Equation (26) into Equation (19), the parameter K_{p0} is evaluated as:

$$K_{p0} = |\alpha|/\left(\frac{\mu^{cs}-m}{\mu-m} - 1\right)\left(\left(D_t\frac{d\varepsilon_t}{d\tau}\right) - 1\right) \qquad (27)$$

There are two methods to determine b_{r1} and b_{r2}. (These parameters are mainly relevant for cyclic loading.) First, by evaluating the particle breakage index (B_r) and total plastic work (W_p) in different cycles of an interface shear test, the parameters b_{r1} and b_{r2} are obtained by fitting a hyperbolic curve between B_r and W_p. The second method employs trial and error, such that the model prediction in the plane of u_n-u_t matches the corresponding cyclic experimental data.

It is worth mentioning that only a single set of model parameters is needed to simulate the behaviour of axially loaded piles in granualar soils with different densities and under different soil confinement pressures subjected to both monotonic and cyclic loading.

4 NUMERICAL PREDICTIONS

Here, the HWI modeling capabilities are examined using the results of centrifuge pile tests by Fioravante (2002) and interface shear tests by Wang et al. (2020).

4.1 Monotonic sand-pile behavior

Fioravante (2002) conducted a series of centrifuge tests on axially loaded aluminum alloy piles of 6 mm and 10 mm diameter (D) and 245 mm length (L) with different surface roughness (R_n=0.01, 0.06, and 0.45) buried in Toyoura sand. The properties of the Toyoura sand are presented in Table 2; φ_{cv} in the table is the constant volume friction angle. The centrifuge acceleration was set to 30g, 50g, 80g and 133g to reproduce the conditions of two prototype piles with D=0.3 m and L~8m, and D=0.8 m and L~20m. Direct shear tests were also performed between the Toyoura sand and the aluminum pile material with different surface roughness (R_n=0.01, 0.13, and 0.25) and normal stiffness (K) (Fioravante, 2002; Ghionna and Mortara, 2002). In the current study, the centrifuge tested piles were simulated by the HWI model at prototype scale. The interface model in the HWI modeling was calibrated using the interface shear test data from Fioravante (2002) for three surface roughness values. The calibrated interface model parameters from Table 3, were used in HWI model to predict the tests by Fioravante (2002).

Table 2. Properties of sandy soils

Soil	Dr (%)	D_{50} (mm)	Max. void ratio, e_{max}	Min. void ratio, e_{min}	φ_{cv} (°)
Toyoura	~90	0.22	1.024	0.64	31.6
Medium fine	60	0.28	0.905	0.454	37

The model predictions for the interface shear tests between the Toyoura sand and the aluminum surface with different roughness (R_n=0.01 and 0.13) under various normal stiffness are illustrated in Figure 2. As can be seen, the model reproduces the experimental observations very well. The HWI model predictions for the pile tests with different dimensions and surface roughness (R_n=0.01, 0.06, and 0.45) are also shown in Figure 3. As can be observed, there are good agreements between the numerical predictions and the laboratory test data. It is

worth noting that in the HWI modelling, the values of the constitutive model parameters for R_n=0.06 was simply linearly interpolated between the input values used for R_n=0.06 and R_n=0.13. Moreover, the calibration parameters for R_n=0.45 was assumed to be the same as R_n=0.25 as they are higher than R_{cr} (R_{cr}=0.13 is assumed in this study).

Table 3. Constitutive model input parameters

Symbol	Fioravante (2002)			Wang et al. (2020)
	R_n=0.01	R_n=0.13	R_n=0.25	R_n=rough
D_{t0} *(MPa)*	1.6	1.6	1.6	0.5
D_{n0}*(MPa)*	2.2	2.2	2.2	0.6
μ^{cs}	0.32	0.63	0.66	0.56
e_{cs0}	0.72	0.91	0.95	0.6
λ	0.17	0.13	0.075	0.02
A^d	5	5	5	0.21
K^d	0.7	0.3	0.3	16
K^f	0	2.3	2.1	1
K_{p0}	0.15	0.15	0.15	0.1
b_{r1} *(MPa)*	N/A	N/A	N/A	1.2
b_{r2}	N/A	N/A	N/A	1.2

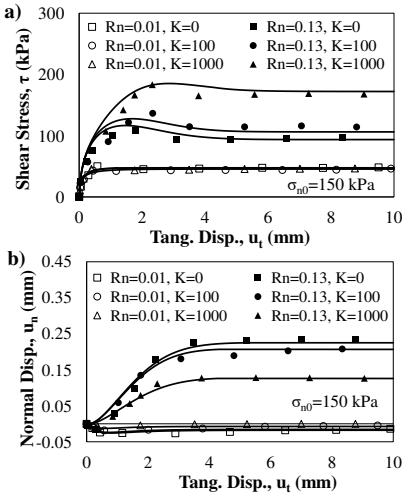

Figure 2. Model predictions against test data (Fioravante, 2002) for different K (kPa/mm) and R_n; a) τ-u_t, and b) u_t-u_n.

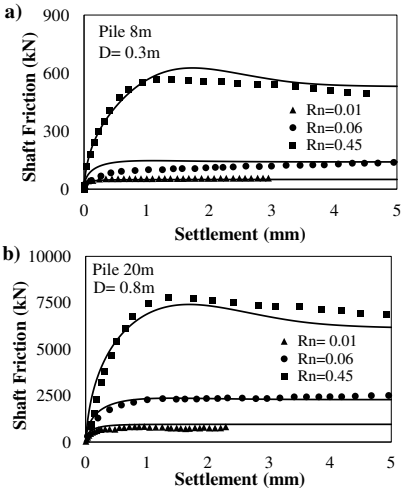

Figure 3. Model predictions against centrifuge data (Fioravante, 2002) for different R_n; a) 8m pile and b) 20m pile.

4.2 Cyclic sand -pile behavior

Wang et al. (2020) designed a ring shear test apparatus under CNS conditions to reproduce the conditions of a steel pile with D=1.8m at different depths up to 30m in a saturated medium fine sand (Table 2) under cyclic loading. Thus, in the current study, a pile with 30m length was simulated by the HWI model. The constitutive model parameters and the boundary input conditions are listed in Table 3 and Table 4 respectively. The numerical predictions of shear stress at 5m and 20m depths are presented in Figure 4 and Figure 5 respectively compared to laboratory tests.

Table 4. Boundary conditions for the cyclic tests

Depth (m)	K(kPa/mm)	Initial normal stress σ_{n0} (kPa)
5	142	50
20	284	200

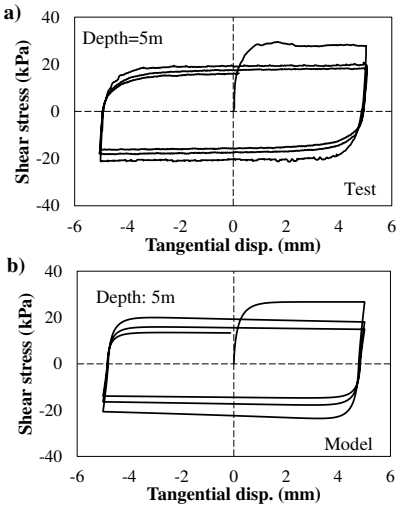

Figure 4. Model predictions against test data (Wang et al., 2020) for a pile at depth=5m; a) test data and b) HWI model.

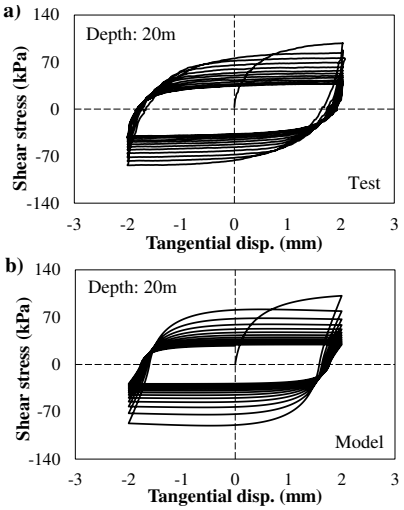

Figure 5. Model predictions against test data (Wang et al., 2020) for a pile at depth=20m; a) test data and b) HWI model.

As can be seen from the figures, the pile model simulated with the HWI approach predicts very well the cyclic tests data under different loading amplitudes (i.e. 5mm and 2mm). The model also simulates nicely the

cyclic stress degradation phenomenon in axially loaded piles. The stress stabilization after several cycles is also well captured by the HWI model as shown in Figure 5.

5 CONCLUSIONS

In this study, a 'Hybrid-Winkler-Interface' (HWI) model for axially loaded piles was developed, and the numerical simulation and calibration process were described. The measurements obtained from the centrifuge and shear tests were used to validate and evaluate the capability of the developed HWI model to predict complex soil-pile interaction behaviours under monotonic and cyclic loading. The numerical simulations shows that the HWI model is an efficient technique to simulate accurately the hardening/softening and cyclic stress degradation behaviours in shaft resistance response. In addition, it addresses very well the effect of compaction/dilation behaviours in granular adjacent soils on the soil-pile friction. The HWI was also able to capture the effect of surface roughness on the shaft resistance in axially loaded piles. It should be noted that this modelling approach simulates the whole complex stress-displacement relationship and volumetric behaviours under different normal stresses, densities and normal stiffness with only a single set of model parameters under both monotonic and cyclic loading conditions.

6 ACKNOWLEDGEMENTS

The authors are grateful to Prof. Charles-Darwin Annan from Université Laval for his invaluable insights.

7 REFERENCES

API. 2007. *2A-WSD-Recommended Practice for Planning, Designing and Constructing Fixed Offshore Platforms-Working Stress Design*. American Petroleum Institute.

Boulon, M., Foray, P. 1986. Physical and numerical simulation of lateral shaft friction along offshore piles in sand. *3rd Int. Conf. Numer. Methods Offshore Piling, Paris, Fr.*, 127–148.

Dassault Systèmes. 2014. *Abaqus User Subroutines Reference Guide*.

Fioravante, V. 2002. On the shaft friction modeling of non-displacement piles in sand, *Soils Found* **42**, 23–33.

Ghionna, V. N., Mortara, G. 2002. An elastoplastic model for sand—structure interface behaviour. *Géotechnique* **52**, 41–50.

Han, F., Salgado, R., Prezzi, M., Lim, J. 2017. Shaft and base resistance of non-displacement piles in sand. *Comput. Geotech.* **83**, 184–197.

Hardin, B. O., Richart, F. E. J. 1963. Elastic Wave Velocities in Granular Soils. *J. Soil Mech. Found. Div.* **89**, 33–65.

Houlsby, G. T. 1991. How the dilatancy of soils affects their behavior. *Proc. the10th Eur. Conf. Soil Mech. Found. Eng. Florence*, 1189–1202. Oxford: Univeristy of Oxford.

Jardine, R. J., Overy, R. F., Chow, F. C. 1998. Axial Capacity of Offshore Piles in Dense North Sea. *J. Geotech. Geoenvironmental Eng.* **124**, 171–178.

Jardine, R. J., Standing, J. R. 2012. Field axial cyclic loading experiments on piles driven in sand. *Soils Found.* **52** (4), 723–736.

Kraft, L. M., Ray, R. P., Kagawa, T. 1981. Theoretical t-z Curves. *J. Geotech. Eng. Div.* **107** (11), 1543–1561.

Kulhawy, F. H. 1991. Drilled Shaft Foundations. *Found. Eng. Handb.* (Ed: Fang, H.Y.), 537–552.

Lashkari, A. 2013. Prediction of the shaft resistance of nondisplacement piles in sand. *Int. J. Numer. Anal. Methods Geomech.* **37** (8), 904–931.

Lehane, B. M., Gaudin, C., Schneider, J. A. 2005. Scale effects on tension capacity for rough piles buried in dense sand. *Géotechnique* **55** (10), 709–719.

Loukidis, D., Salgado, R. 2008. Analysis of the shaft resistance of non-displacement piles in sand. *Géotechnique* **58** (4), 283–296.

Merritt, A., Schroeder, F., Jardine, R., Stuyts, B., Cathie, D., Cleverly, W. 2012. Development of pile design methodology for an offshore wind farm in the north sea. *Offshore Site Investig. Geotech. Integr. Technol. Futur.*

Randolph, M. F. 2003. Science and empiricism in pile foundation design. *Geotechnique* **53** (10), 847–875.

Randolph, M. F., Wroth, C. P. 1978. Analysis of deformation of vertically loaded piles. *J. Geotech. Eng. Div.* **104** (12), 1465–1488.

Rollins, K. M., Clayton, R. J., Mikesell, R. C., Blaise, B. C. 2005. Drilled Shaft Side Friction in Gravelly Soils. *J. Geotech. Geoenviron. Eng.* **131** (8), 987–1003.

Saberi, M., Annan, C.D., Konrad, J.M. 2017. Constitutive Modeling of Gravelly Soil-Structure Interface Considering Particle Breakage. *J. Eng. Mech.* **143** (8).

Saberi, M., Annan, C.D., Konrad, J.M. 2018. On the mechanics and modeling of interfaces between granular soils and structural materials. *Arch. Civ. Mech. Eng.* **18** (4), 1562–1579.

Saberi, M., Annan, C.D., Konrad, J.M. 2019. Implementation of a soil-structure interface constitutive model for application in geo-structures. *Soil Dyn. Earthq. Eng.* **116**.

Saberi, M., Annan, C.D., Konrad, J.M. 2020a. A non-linear interface model for monotonic shear coupling in granular soil-structure interaction problems. *Géotechnique Lett.* **10** (2), 336–345.

Saberi, M., Annan, C.D., Konrad, J.M. 2020b. Three-dimensional constitutive model for cyclic behavior of soil-structure interfaces. *Soil Dyn. Earthquake Eng.* **134**.

Saberi, M., Annan, C.D., Sheil, B. B. 2022. An efficient numerical approach for simulating soil-pipe interaction behaviour under cyclic loading. *Comput. Geotech.* **146**.

Uesugi, M., Kishida, H. 1986. Frictional resistance at yield between dry Sand and mild Steel. *Soils Found.* **26** (4), 139–149.

Vafaei, N., Fakharian, K. Sadrekarimi, A. 2021. Sand-sand and sand-steel interface grain-scale behavior under shearing. *Transp. Geotech.* **30**.

Wang, L., Zhou, W., Guo, Z., Rui, S. 2020. Frequency change and accumulated inclination of offshore wind turbine jacket structure with piles in sand under cyclic loadings. *Ocean Eng.* **217**.

Zhou, W., Wang, L., Guo, Z., Liu, J., Rui, S. 2019. A novel t-z model to predict the pile responses under axial cyclic loadings. *Comput. Geotech.* **112**, 120–134.